Int J Adv Manuf Technol (2010) 46:91–99
DOI 10.1007/s00170-009-2081-0

ORIGINAL ARTICLE

The actual geometry of the cutting tool involved in machining

Z. Y. Shi · Z. Q. Liu

Received: 5 January 2009 / Accepted: 28 April 2009 / Published online: 17 May 2009
© Springer-Verlag London Limited 2009

Abstract Understanding actual geometry of the cutting tool involved in machining is critical to the investigation of the mechanism of cutting process. According to control pattern of the flank and the insert shape, the cutting tools are classified into four different types in this paper including S- and non-S-shaped tools with cylindrical control and conical control. By establishing all the four kinds of tools' 3-D models, the actual geometry of the cutting tool can be obtained. Research results suggest that the actual geometry involved in machining of the S-shaped inserts whether with cylindrical control or conical control is sphere; non-S-shaped with cylindrical control tools is ellipsoid while non-S-shaped with conical control is paraboloid.

Keywords Cylindrical control · Conical control · Tool shape · Actual geometry

List of symbols

A	one point around tool nose
A_0	projection of point A in XOY plane
A_1	projection of point A in $X_1O_1Y_1$ plane
A_2	projection of point A in $X_2O_2Y_2$ plane
β	the angle between OA_0 and OX
R	the cutting tool nose radius
k	coordinate of point A in Z direction in O-XYZ coordinate system
l	the thickness of the cutting tool
C	C-shaped tools that means that the angle of tool nose is 80°
D	D-shaped tools that means that the angle of tool nose is 55°
K	K-shaped tools that means that the angle of tool nose is 55°
V	V-shaped tools that means that the angle of tool nose is 35°
W	W-shaped tools that means that the angle of tool nose is 80°
T	T-shaped tools that means that the angle of tool nose is 60°
S	S-shaped tools that means that the angle of tool nose is 90°
x	coordinate of point A in X direction in O-XYZ coordinate system
r_1	the major cutting edge radius
y	coordinate of point A in Y direction in O-XYZ coordinate system
z	coordinate of point A in Z direction in O-XYZ coordinate system
x_1	coordinate of point A in X_1 direction in O_1-$X_1Y_1Z_1$ coordinate system
y_1	coordinate of point A in Y_1 direction in O_1-$X_1Y_1Z_1$ coordinate system
z_1	coordinate of point A in Z_1 direction in O_1-$X_1Y_1Z_1$ coordinate system
x_2	coordinate of point A in X_2 direction in O_2-$X_2Y_2Z_2$ coordinate system
y_2	coordinate of point A in Y_2 direction in O_2-$X_2Y_2Z_2$ coordinate system
z_2	coordinate of point A in Z_2 direction in O_2-$X_2Y_2Z_2$ coordinate system
v_1	the angle between Y_1O_1 and O_1A_1
m	the length of the major cutting edge

Z. Y. Shi (✉) · Z. Q. Liu
School of Mechanical Engineering, Shandong University, Jinan 250061, China
e-mail: zhenyushi@qq.com

Z. Q. Liu
e-mail: melius@sdu.edu.cn

M_1 transformation matrix from O_1-$X_1Y_1Z_1$ to O-XYZ
V_2 the angle between O_2Z_2 and O_2A_2
n the length of the minor cutting edge
r_2 the minor cutting edge radius
M_2 transformation matrix from O_2-$X_2Y_2Z_2$ to O-XYZ
Q from coordinate system O-XYZ to O_1-$X_1Y_1Z_1$, translations Q units along Y direction
P from coordinate system O-XYZ to O_2-$X_2Y_2Z_2$, translations P units along X direction
t matrix parameter
ε_r tool nose angle
θ rotate angle
ω half top angle of the control cone

1 Introduction

With increased emphasis on manufacturing, understanding the machining mechanism assumes great significance [1–5]. An important aspect of machining mechanism is the presence of the effect of the cutting tool geometry. The recent research in the effects of cutting tool geometry concentrates on studying the cutting edge [6, 7] and tool nose [8–11]. A number of researchers have analyzed the effect of the cutting tool geometry in machining either by cutting experiments [12, 13] or finite element method (FEM) simulations [14, 15]. Rech et al. [16] tested the behavior of coated PM-HSS milling inserts with different edge radius and concluded that the modifications of the cutting edge radius are the main criteria influencing the wear resistance. Chou and Evans [17] found that the distance from the cutting edge to the nominal machined surface changes is the main reason of the size effect of cutting force. Ceretti et al. [18] used DEFORM 2D software to simulate orthogonal cutting operation by changing the tool geometry and cutting speed. Li and Shih [19] used the Third Wave AdvantEdge machining simulation software to simulate the effects of cutting speed and cutting edge radius on cutting forces, chip thickness and tool temperature. These researches investigated the effect of the cutting tool geometry either from the tool edge or from the tool nose, but none of them had considered the two aspects comprehensively.

In actual cutting, especially in micromachining, the metal removal rate is very little. The major cutting edge and the minor cutting edge as well as the tool nose are all involved in microcutting processes, so it is important to study the actual geometry of the cutting tool involved in machining. This paper develops the model of the actual geometry of the cutting tool involved in machining using mathematic analysis method based on the insert shape and the control pattern of the flank including cylindrical control and conical control.

The relationship between the major cutting edge and the minor cutting edge is used to define the insert shape. The insert shape is represented as S according to ISO code when tool nose angle is 90°. The insert, otherwise, is designated as non-S-shaped. In this paper, four different 3-D models including S- and non-S-shaped tools with cylindrical control and conical control are established based on the flank face and the insert shape.

2 Three-dimension geometrical modeling

In traditional machining, only the primary cutting edge is mainly participated in cutting process. However, the whole nose of the cutting tool is participated in microcutting process due to the very little metal removal. Thus, the actual geometry involved in microcutting is determined by the major cutting edge, the minor cutting edge, and the third edge called backside cutting edge as shown in Fig. 1. It is necessary to develop the model of the actual geometry involved in machining to better understand the effects of tool geometry on cutting process.

According to the control model of the flank, the cutting tool can be classified into cylindrical control and conical control, as shown in Figs. 2 and 3.

When the cutting tool is with cylindrical control, the center of the tool nose is taken as the coordinate origin O, and the coordinate system O-XYZ can be established. Point A at backside edge can be expressed in Eq. 1.

$$A(\beta,k)=\left\{\begin{array}{c} x=R\cos\beta \\ y=R\sin\beta \\ z=-k \end{array}\right\} \tag{1}$$

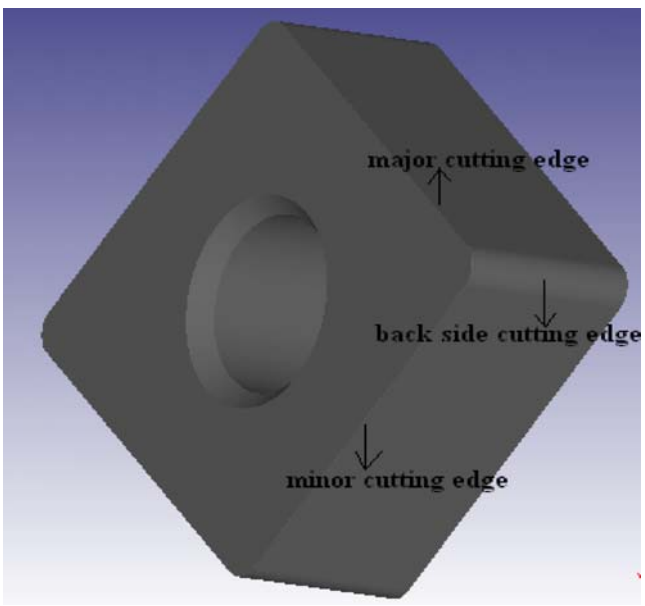

Fig. 1 3-D cutting tool model

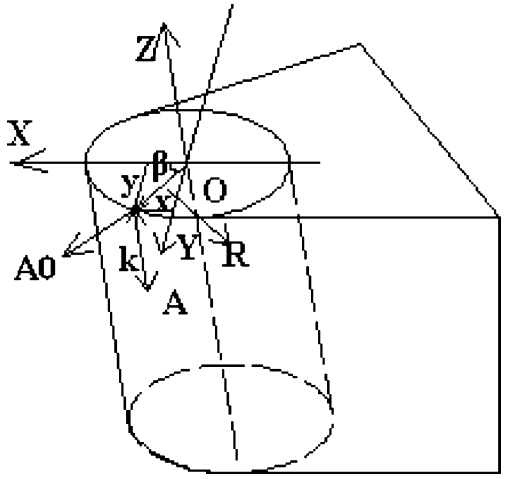

Fig. 2 Cylindrical control cutting tool

where $0<k<l$; l is the insert thickness; R is the nose radius, β is the angle between OA_0 and OX; A_0 is the projection of point A in XOY plane.

When the tool is with conical control, point A can be expressed in Eq. 2,

$$A(\beta,k)=\left\{\begin{array}{c} x=(R-ktg\omega)\cos\beta \\ y=(R-ktg\omega)\sin\beta \\ z=-k \end{array}\right\} \tag{2}$$

where ω is the half top angle of the cone.

The S-shaped and non-S-shaped inserts with cylindrical control tools and conical control tools are classified as shown in Table 1.

In Table 1, according to ISO code, when the insert is C- or W-shaped, the tool nose angle ε_r is 80°; when the insert is D- or K-shaped, ε_r is 55°; when the insert is V-shaped, ε_r is 35°; when the insert is D-shaped, ε_r is 55°; when the insert is T-shaped, ε_r is 60°.

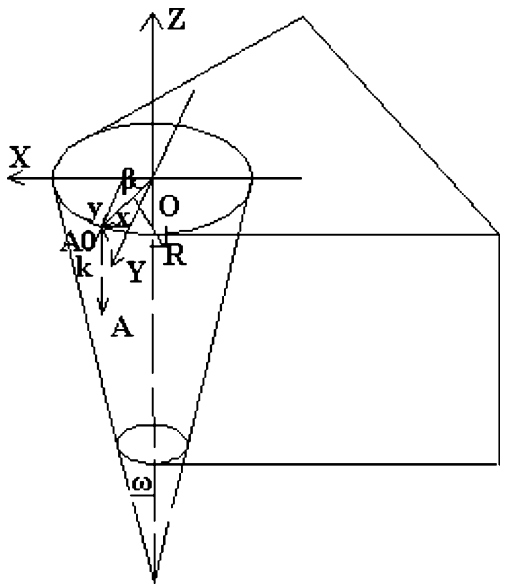

Fig. 3 Conical control cutting tool

In micromachining, the metal removal is very little, and the feed rate is almost equal to the cutting edge radius. Thus, it is not suitable to take the cutting edge to be sharp-edged; the cutting edge radius has to be considered [20]. The schematic diagram of the major cutting edge can be seen in Fig. 4. Because the intersecting line between the round edge of the cutting tool and the cross section is circular, so point A at major cutting edge in coordinate system O_1-$X_1Y_1Z_1$ can be expressed in Eq. 3

$$A(\beta_1,u_1)=\begin{bmatrix} x_1 \\ y_1 \\ z_1 \end{bmatrix}=\begin{bmatrix} u_1 \\ -r_1\cos\beta_1 \\ r_1\sin\beta_1 \end{bmatrix} \tag{3}$$

where $0<u_1<m$; m is the length of the major cutting edge; r_1 is the major cutting edge radius; β_1 is the angle between $Y_1O_1$and O_1A_1; A_1 is the projection of point A in $X_1O_1Y_1$ plane

Supposing the transformation matrix from the coordinate system O_1-$X_1Y_1Z_1$ to the coordinate system O-XYZ is M_1, the major cutting edge in coordinate system O-XYZ can be represented in Eq. 4:

$$\begin{bmatrix} x \\ y \\ z \\ t \end{bmatrix}=M_1\cdot\begin{bmatrix} x_1 \\ y_1 \\ z_1 \\ t \end{bmatrix}=M_1\cdot\begin{bmatrix} u_1 \\ -r_1\cos\beta_1 \\ r_1\sin\beta_1 \\ t \end{bmatrix} \tag{4}$$

where t is matrix parameter

Meanwhile, point A at minor cutting edge in coordinate system O_2-$X_2Y_2Z_2$ can be expressed in Eq. 5 according to the schematic diagram of the minor cutting edge in Fig. 5.

$$A(\beta_2,u_2)=\begin{bmatrix} x_2 \\ y_2 \\ z_2 \end{bmatrix}=\begin{bmatrix} -r_2\cos\beta_2 \\ u_2 \\ r_2\sin\beta_2 \end{bmatrix} \tag{5}$$

where $0<u_2<n$; n is the length of the minor cutting edge; r_2 is the minor cutting edge radius; β_2 is the angle between O_2Z_2 and O_2A_2; A_2 is the projection of point A in $X_2O_2Y_2$ plane

The transformation matrix from the coordinate system O_2-$X_2Y_2Z_2$ to the coordinate system O-XYZ is supposed to be M_2; the minor cutting edge in coordinate system O-XYZ can be represented in Eq. 6:

$$\begin{bmatrix} x \\ y \\ z \\ t \end{bmatrix}=M_2\cdot\begin{bmatrix} x_2 \\ y_2 \\ z_2 \\ t \end{bmatrix}=M_2\cdot\begin{bmatrix} -r_2\cos\beta_2 \\ u_2 \\ r_2\sin\beta_2 \\ t \end{bmatrix} \tag{6}$$

Table 1 Tool types

Control model of flank face	Cylindrical control
	Conical control
Insert shape	S shape
	Non-S-shape (including C, D, K, V, W, T)

Now, the tool nose, the major cutting edge, and the minor cutting edge are all in the same coordinate system O-XYZ. By solving Eqs. 1, 4, and 6 or Eqs. 2, 4, and 6, the actual geometry involved in machining can be obtained.

3 Determination of transformation matrix

When the insert shape is S, the major cutting edge is perpendicular to the minor cutting edge. The coordinate system O_1-$X_1Y_1Z_1$ represented the major cutting edge which can be regarded as the coordinate system O-XYZ with translating Q units along Y-axis direction as shown in Fig. 6, so the transformation matrix M_1 from O_1-$X_1Y_1Z_1$ to O-XYZ can be expressed in Eq. 7,

$$M_1 = \begin{bmatrix} 1 & 0 & 0 & 0 \\ 0 & 1 & 0 & y_0 \\ 0 & 0 & 1 & 0 \\ 0 & 0 & 0 & 1 \end{bmatrix} \tag{7}$$

Then, Eq. 4 can be rewritten as Eq. 8:

$$\begin{bmatrix} x \\ y \\ z \\ t \end{bmatrix} = M_1 \cdot \begin{bmatrix} u_1 \\ -r_1\cos\beta_1 \\ r_1\sin\beta_1 \\ t \end{bmatrix} = \begin{bmatrix} 1 & 0 & 0 & 0 \\ 0 & 1 & 0 & y_0 \\ 0 & 0 & 1 & 0 \\ 0 & 0 & 0 & 1 \end{bmatrix} \cdot \begin{bmatrix} u_1 \\ -r_1\cos\beta_1 \\ r_1\sin\beta_1 \\ t \end{bmatrix} = \begin{bmatrix} u_1 \\ -r_1\cos\beta_1 + y_0 t \\ r_1\sin\beta_1 \\ t \end{bmatrix} \tag{8}$$

where $y_0 t = Q$

Meanwhile, the coordinate system O_2-$X_2Y_2Z_2$ represented the minor cutting edge which can be regarded as the coordinate system O-XYZ by translating P units along X-axis direction as shown in Fig. 7, so the transformation matrix M_2 from O_2-$X_2Y_2Z_2$ to O-XYZ can be expressed in Eq. 9, and the minor cutting edge expressed in Eq. 6 in coordinate system O-XYZ can also be rewritten as Eq. 10:

$$M_2 = \begin{bmatrix} 1 & 0 & 0 & x_0 \\ 0 & 1 & 0 & 0 \\ 0 & 0 & 1 & 0 \\ 0 & 0 & 0 & 1 \end{bmatrix} \tag{9}$$

$$\begin{bmatrix} x \\ y \\ z \\ t \end{bmatrix} = \begin{bmatrix} 1 & 0 & 0 & x_0 \\ 0 & 1 & 0 & 0 \\ 0 & 0 & 1 & 0 \\ 0 & 0 & 0 & 1 \end{bmatrix} \begin{bmatrix} -r_2\cos\beta_2 \\ u_2 \\ r_2\sin\beta_2 \\ t \end{bmatrix} = \begin{bmatrix} -r_2\cos\beta_2 + x_0 t \\ u_2 \\ r_2\sin\beta_2 \\ t \end{bmatrix} \tag{10}$$

where $x_0 t = P$

When the insert is non-S-shaped, the tool nose angle is ε_r; then, the coordinate systems O_1-$X_1Y_1Z_1$ compared to the coordinate system O-XYZ need to rotate $\theta = \frac{\pi - \varepsilon_r}{2}$ degrees along Z-axis. According to Fig. 8, the transformation matrix M_1 from O_1-$X_1Y_1Z_1$ to O-XYZ can be expressed in Eq. 11:

$$M_1 = \begin{bmatrix} \cos\theta & -\sin\theta & 0 \\ \sin\theta & \cos\theta & 0 \\ 0 & 0 & 1 \end{bmatrix} \tag{11}$$

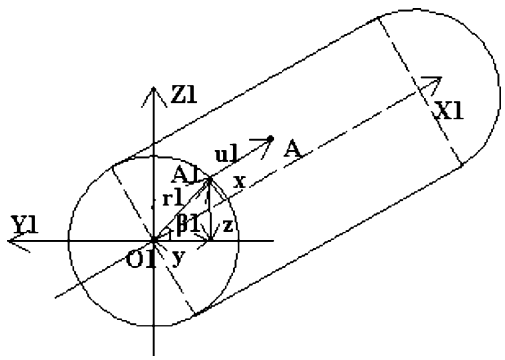

Fig. 4 Schematic diagram of major cutting edge

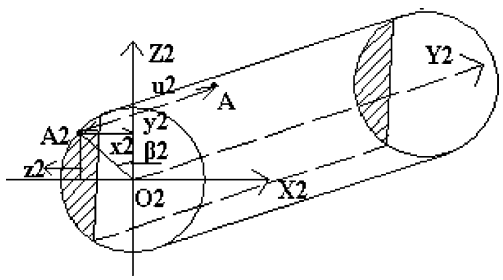

Fig. 5 Schematic diagram of minor cutting edge

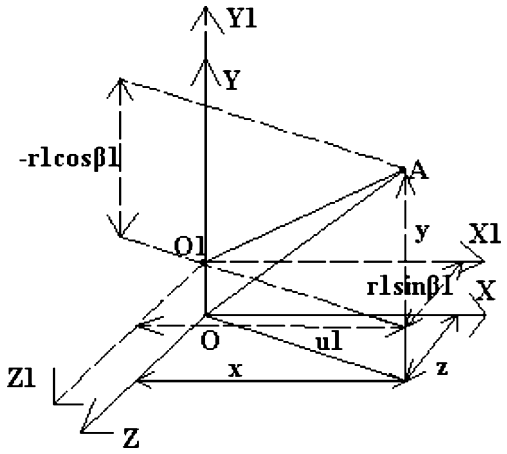

Fig. 6 Coordinate translation in Y direction

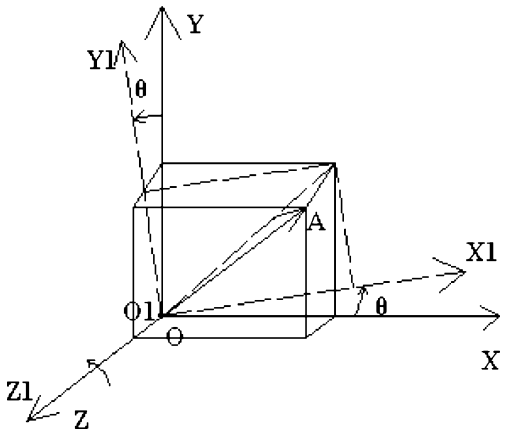

Fig. 8 Coordinate transformation of rotation around Z-axis

Based on Eq. 11, the matrix M_1 can be written as:

$$M_1 = \begin{bmatrix} \sin\frac{\varepsilon_r}{2} & -cos\frac{\varepsilon_r}{2} & 0 \\ \cos\frac{\varepsilon_r}{2} & \sin\frac{\varepsilon_r}{2} & 0 \\ 0 & 0 & 1 \end{bmatrix} \tag{12}$$

The major cutting edge in coordinate system O-XYZ now has been changed as follows:

$$\begin{bmatrix} x \\ y \\ z \end{bmatrix} = \begin{bmatrix} \sin\frac{\varepsilon_r}{2} & -cos\frac{\varepsilon_r}{2} & 0 \\ \cos\frac{\varepsilon_r}{2} & \sin\frac{\varepsilon_r}{2} & 0 \\ 0 & 0 & 1 \end{bmatrix} \cdot \begin{bmatrix} u_1 \\ -r_1\cos\beta_1 \\ r_1\sin\beta_1 \end{bmatrix} \tag{13}$$

$$= \begin{bmatrix} u_1\sin\frac{\varepsilon_r}{2} + r_1\cos\beta_1\cos\frac{\varepsilon_r}{2} \\ u_1\cos\frac{\varepsilon_r}{2} - r_1\cos\beta_1\sin\frac{\varepsilon_r}{2} \\ r_1\sin\beta_1 \end{bmatrix}$$

The coordinate system O_2-$X_2Y_2Z_2$ compared to the coordinate system O-XYZ need to rotate $-\frac{\pi-\varepsilon_r}{2}$ degree along the Z-axis. The transformation matrix M_2 from O_2-$X_2Y_2Z_2$ to O-XYZ can be expressed in Eq. 14, and the minor cutting edge expressed in coordinate system O-XYZ has been changed from Eqs. 10 to 15:

$$M_2 = \begin{bmatrix} \sin\frac{\varepsilon_r}{2} & cos\frac{\varepsilon_r}{2} & 0 \\ -\cos\frac{\varepsilon_r}{2} & \sin\frac{\varepsilon_r}{2} & 0 \\ 0 & 0 & 1 \end{bmatrix} \tag{14}$$

$$\begin{bmatrix} x \\ y \\ z \end{bmatrix} = \begin{bmatrix} \sin\frac{\varepsilon_r}{2} & cos\frac{\varepsilon_r}{2} & 0 \\ -\cos\frac{\varepsilon_r}{2} & \sin\frac{\varepsilon_r}{2} & 0 \\ 0 & 0 & 1 \end{bmatrix} \begin{bmatrix} -r_2\cos\beta_2 \\ u_2 \\ r_2\sin\beta_2 \end{bmatrix} \tag{15}$$

$$= \begin{bmatrix} u_2\cos\frac{\varepsilon_r}{2} - r_2\cos\beta_2\sin\frac{\varepsilon_r}{2} \\ u_2\sin\frac{\varepsilon_r}{2} + r_2\cos\beta_2\cos\frac{\varepsilon_r}{2} \\ r_2\sin\beta_2 \end{bmatrix}$$

The actual geometry involved in machining can be known by solving the system of equations. If the tool is cylindrical control with S shape, the system of equations to be solved is Eqs. 1, 8, and 10. While if the tool is cylindrical control with non-S shape, the system of equations to be solved is Eqs. 1, 13, and 15; conical control with S-shaped tool needs to solve Eqs. 2, 8, and 10 to get the actual geometry, and conical control with non-S-shaped tool needs to solve Eqs. 2, 13, and 15 to get the actual geometry. Table 2 shows the corresponding relationship between the tool types and the system equations to be solved.

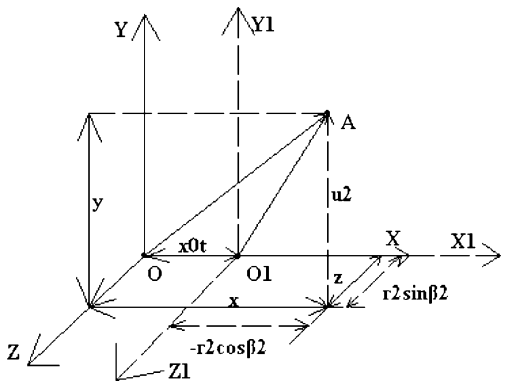

Fig. 7 Coordinate translation in X direction

4 Solving process

4.1 S-shaped tools

For S-shaped tools with cylindrical control or with conical control, the solving processing is similar. By solving the equation groups Eqs. 1, 8, and 10, the following relation-

Table 2 Tool types vs equations to be solved

Tool types	System equations to be solved
Cylindrical control with S-shaped tool	Eqs. 1, 8, and 10
Cylindrical control with non-S-shaped tool	Eqs. 1, 13, and 15
Conical control with S-shaped tool	Eqs. 2, 8, and 10
conical control with non-S-shaped tool	Eqs. 2, 13, and 15

ship can be gotten in Eq. 16, because $r_1 \cos v_1 = Q - y$, $r_2 \cos v_2 = P - x$; Eq. 16 can also be written as shown in Eq. 17; from that, the geometry established by the major cutting edge, the minor cutting edge, and the backside cutting edge is finally determined to be a sphere with the center of the sphere at point ($\frac{P}{2}$, $\frac{Q}{2}$,0).

In the same way, by solving the equation groups Eqs. 2, 8, and 10, the relationship shown in Eq. 18 can also be obtained and the actual geometry for S-shaped tools with conical control is sphere too.

$$\begin{aligned} 3x^2 + 3y^2 + 3z^2 = {} & R^2 + k^2 + u_1^2 + r_1^2 + Q^2 \\ & - 2Qr_1 \cos\beta_1 + u_2^2 + r_2^2 + P^2 \\ & - 2Pr_2 \cos\beta_2 \end{aligned} \tag{16}$$

$$\begin{aligned} & \left(x - \frac{P}{2}\right)^2 + \left(y - \frac{Q}{2}\right)^2 + z^2 \\ & = \frac{R^2 + r_1^2 + r_2^2}{2} - \frac{Q^2 + P^2}{4} \end{aligned} \tag{17}$$

$$\begin{aligned} & \left(x - \frac{P}{2}\right)^2 + \left(y - \frac{Q}{2}\right)^2 + \left[z - \left(\frac{tg^2\omega}{4} - \frac{Rtg\omega}{2}\right)\right]^2 \\ & = \frac{R^2 + r_1^2 + r_2^2}{2} + \frac{P^2 + Q^2}{4} + \left(\frac{tg^2\omega}{4} - \frac{Rtg\omega}{2}\right)^2 \end{aligned} \tag{18}$$

4.2 Non-S-shaped tools

For non-S-shaped tools, the first step of solving process is similar to S-shaped tools, and, by solving Eqs. 1, 3, and 15, the following relationship for cylindrical control tools can be obtained:

$$x^2 + y^2 + z^2 = \frac{r_1^2 + r_2^2 + R^2}{3} + \frac{u_1^2 + u_2^2 + k^2}{3} \tag{19}$$

It can also be written as:

$$\begin{cases} x^2 + y^2 = \frac{r_1^2 + r_2^2 + R^2}{3} + \frac{u_1^2 + u_2^2 - 2k^2}{3} \\ z = k \end{cases} \tag{20}$$

In Eq. 20, R, r_1, and r_2 are known as the nose radius, the major cutting edge radius, and the minor cutting edge radius, respectively; only u_1, u_2, and t need to be solved. According to Eqs. 1, 13, and 15, the following linear systems of equations can be obtained:

$$\begin{cases} u_1 \sin\frac{\varepsilon_r}{2} + r_1 \cos\beta_1 \cos\frac{\varepsilon_r}{2} - u_2 \cos\frac{\varepsilon_r}{2} - r_2 \cos\beta_2 \sin\frac{\varepsilon_r}{2} = 0 \\ u_1 \sin\frac{\varepsilon_r}{2} + r_1 \cos\beta_1 \cos\frac{\varepsilon_r}{2} = R\cos\beta \\ u_1 \cos\frac{\varepsilon_r}{2} - r_1 \cos\beta_1 \sin\frac{\varepsilon_r}{2} - u_2 \sin\frac{\varepsilon_r}{2} + r_2 \cos\beta_2 \cos\frac{\varepsilon_r}{2} = 0 \\ u_1 \cos\frac{\varepsilon_r}{2} - r_1 \cos\beta_1 \sin\frac{\varepsilon_r}{2} = R\sin\beta \end{cases} \tag{21}$$

Assuming sin β and cos β are known, by using Cramer law as shown in Eq. 22, the variables u_1, u_2, cos β_1, and cos β_2 can be solved.

$$x_i = \frac{D_{x_i}}{D} \quad (i = 1, 2, \ldots n) \tag{22}$$

where in Eq. 22:

$$D = \begin{vmatrix} \sin\frac{\varepsilon_r}{2} & r_1\cos\frac{\varepsilon_r}{2} & -r_2\sin\frac{\varepsilon_r}{2} & -\cos\frac{\varepsilon_r}{2} \\ \sin\frac{\varepsilon_r}{2} & r_1\cos\frac{\varepsilon_r}{2} & 0 & 0 \\ \cos\frac{\varepsilon_r}{2} & -r_1\sin\frac{\varepsilon_r}{2} & r_2\cos\frac{\varepsilon_r}{2} & -\sin\frac{\varepsilon_r}{2} \\ \cos\frac{\varepsilon_r}{2} & -r_1\sin\frac{\varepsilon_r}{2} & 0 & 0 \end{vmatrix} = r_1 r_2 \tag{23}$$

$$D_{u_1} = \begin{vmatrix} 0 & r_1\cos\frac{\varepsilon_r}{2} & -r_2\sin\frac{\varepsilon_r}{2} & -\cos\frac{\varepsilon_r}{2} \\ R\cos\beta & r_1\cos\frac{\varepsilon_r}{2} & 0 & 0 \\ 0 & -r_1\sin\frac{\varepsilon_r}{2} & r_2\cos\frac{\varepsilon_r}{2} & -\sin\frac{\varepsilon_r}{2} \\ R\sin\beta & -r_1\sin\frac{\varepsilon_r}{2} & 0 & 0 \end{vmatrix} = Rr_1r_2\left(\cos\frac{\varepsilon_r}{2}\sin\beta + \sin\frac{\varepsilon_r}{2}\cos\beta\right) \tag{24}$$

$$\begin{aligned} D_{u_2} = \begin{vmatrix} \sin\frac{\varepsilon_r}{2} & r_1\cos\frac{\varepsilon_r}{2} & -r_2\sin\frac{\varepsilon_r}{2} & 0 \\ \sin\frac{\varepsilon_r}{2} & r_1\cos\frac{\varepsilon_r}{2} & 0 & R\cos\beta \\ \cos\frac{\varepsilon_r}{2} & -r_1\sin\frac{\varepsilon_r}{2} & r_2\cos\frac{\varepsilon_r}{2} & 0 \\ \cos\frac{\varepsilon_r}{2} & -r_1\sin\frac{\varepsilon_r}{2} & 0 & R\sin\beta \end{vmatrix} &= Rr_1r_2\left(\cos^2\frac{\varepsilon_r}{2} - \sin^2\frac{\varepsilon_r}{2}\right) \\ &\times\left(\cos v\cos\frac{\varepsilon_r}{2} - \sin v\sin\frac{\varepsilon_r}{2}\right) \\ &+ 2Rr_1r_2\sin\frac{\varepsilon_r}{2}\cos\frac{\varepsilon_r}{2} \\ &\left(\cos v\sin\frac{\varepsilon_r}{2} + \sin v\cos\frac{\varepsilon_r}{2}\right) \end{aligned} \tag{25}$$

$$D_{\cos\beta_1} = \begin{vmatrix} \sin\frac{\varepsilon_r}{2} & 0 & -r_2\sin\frac{\varepsilon_r}{2} & -\cos\frac{\varepsilon_r}{2} \\ \sin\frac{\varepsilon_r}{2} & R\cos\beta & 0 & 0 \\ \cos\frac{\varepsilon_r}{2} & 0 & r_2\cos\frac{\varepsilon_r}{2} & -\sin\frac{\varepsilon_r}{2} \\ \cos\frac{\varepsilon_r}{2} & R\sin\beta & 0 & 0 \end{vmatrix} = Rr_2\left(\cos\beta\cos\frac{\varepsilon_r}{2} - \sin\beta\sin\frac{\varepsilon_r}{2}\right) \tag{26}$$

By using Cramer law, u_1, u_2, and cos β_1 can be obtained.

$$u_1 = \frac{D_{u_1}}{D} = \frac{\begin{vmatrix} 0 & r_1\cos\frac{\varepsilon_r}{2} & -r_2\sin\frac{\varepsilon_r}{2} & -\cos\frac{\varepsilon_r}{2} \\ R\cos\beta & r_1\cos\frac{\varepsilon_r}{2} & 0 & 0 \\ 0 & -r_1\sin\frac{\varepsilon_r}{2} & r_2\cos\frac{\varepsilon_r}{2} & -\sin\frac{\varepsilon_r}{2} \\ R\sin\beta & -r_1\sin\frac{\varepsilon_r}{2} & 0 & 0 \end{vmatrix}}{\begin{vmatrix} \sin\frac{\varepsilon_r}{2} & r_1\cos\frac{\varepsilon_r}{2} & -r_2\sin\frac{\varepsilon_r}{2} & -\cos\frac{\varepsilon_r}{2} \\ \sin\frac{\varepsilon_r}{2} & r_1\cos\frac{\varepsilon_r}{2} & 0 & 0 \\ \cos\frac{\varepsilon_r}{2} & -r_1\sin\frac{\varepsilon_r}{2} & r_2\cos\frac{\varepsilon_r}{2} & -\sin\frac{\varepsilon_r}{2} \\ \cos\frac{\varepsilon_r}{2} & -r_1\sin\frac{\varepsilon_r}{2} & 0 & 0 \end{vmatrix}} = R(\cos\frac{\varepsilon_r}{2}\sin\beta + \sin\frac{\varepsilon_r}{2}\cos\beta) \tag{27}$$

$$u_2 = \frac{D_{u_2}}{D} = \frac{\begin{vmatrix} \sin\frac{\varepsilon_r}{2} & r_1\cos\frac{\varepsilon_r}{2} & -r_2\sin\frac{\varepsilon_r}{2} & 0 \\ \sin\frac{\varepsilon_r}{2} & r_1\cos\frac{\varepsilon_r}{2} & 0 & R\cos\beta \\ \cos\frac{\varepsilon_r}{2} & -r_1\sin\frac{\varepsilon_r}{2} & r_2\cos\frac{\varepsilon_r}{2} & 0 \\ \cos\frac{\varepsilon_r}{2} & -r_1\sin\frac{\varepsilon_r}{2} & 0 & R\sin\beta \end{vmatrix}}{\begin{vmatrix} \sin\frac{\varepsilon_r}{2} & r_1\cos\frac{\varepsilon_r}{2} & -r_2\sin\frac{\varepsilon_r}{2} & -\cos\frac{\varepsilon_r}{2} \\ \sin\frac{\varepsilon_r}{2} & r_1\cos\frac{\varepsilon_r}{2} & 0 & 0 \\ \cos\frac{\varepsilon_r}{2} & -r_1\sin\frac{\varepsilon_r}{2} & r_2\cos\frac{\varepsilon_r}{2} & -\sin\frac{\varepsilon_r}{2} \\ \cos\frac{\varepsilon_r}{2} & -r_1\sin\frac{\varepsilon_r}{2} & 0 & 0 \end{vmatrix}} = R\left(\cos^2\frac{\varepsilon_r}{2} - \sin^2\frac{\varepsilon_r}{2}\right) \times (\cos\beta\cos\frac{\varepsilon_r}{2} - \sin\beta\sin\frac{\varepsilon_r}{2}) + 2R\sin\frac{\varepsilon_r}{2}\cos\frac{\varepsilon_r}{2}(\cos\beta\sin\frac{\varepsilon_r}{2} + \sin\beta\cos\frac{\varepsilon_r}{2}) \tag{28}$$

$$\cos\beta_1 = \frac{D_{\cos\beta_1}}{D} = \frac{\begin{vmatrix} \sin\frac{\varepsilon_r}{2} & 0 & -r_2\sin\frac{\varepsilon_r}{2} & -\cos\frac{\varepsilon_r}{2} \\ \sin\frac{\varepsilon_r}{2} & R\cos\beta & 0 & 0 \\ \cos\frac{\varepsilon_r}{2} & 0 & r_2\cos\frac{\varepsilon_r}{2} & -\sin\frac{\varepsilon_r}{2} \\ \cos\frac{\varepsilon_r}{2} & R\sin\beta & 0 & 0 \end{vmatrix}}{\begin{vmatrix} \sin\frac{\varepsilon_r}{2} & r_1\cos\frac{\varepsilon_r}{2} & -r_2\sin\frac{\varepsilon_r}{2} & -\cos\frac{\varepsilon_r}{2} \\ \sin\frac{\varepsilon_r}{2} & r_1\cos\frac{\varepsilon_r}{2} & 0 & 0 \\ \cos\frac{\varepsilon_r}{2} & -r_1\sin\frac{\varepsilon_r}{2} & r_2\cos\frac{\varepsilon_r}{2} & -\sin\frac{\varepsilon_r}{2} \\ \cos\frac{\varepsilon_r}{2} & -r_1\sin\frac{\varepsilon_r}{2} & 0 & 0 \end{vmatrix}} = \frac{R(\cos\beta\cos\frac{\varepsilon_r}{2} - \sin\beta\sin\frac{\varepsilon_r}{2})}{r_1} \tag{29}$$

As known for $k=r_1 \sin \beta_1$, then

$$k^2 = r_1^2 - r_1^2\cos^2\beta_1 = r_1^2 - R^2\left(\cos\beta\cos\frac{\varepsilon_r}{2} - \sin\beta\sin\frac{\varepsilon_r}{2}\right)^2$$

$$\begin{aligned} u_1^2 + u_2^2 - 2k^2 = {} & R^2(\cos\tfrac{\varepsilon_r}{2}\sin\beta + \sin\tfrac{\varepsilon_r}{2}\cos\beta)^2 \\ & + 2\left[r_1^2 - R^2\left(\cos\beta\cos\tfrac{\varepsilon_r}{2} - \sin\beta\sin\tfrac{\varepsilon_r}{2}\right)^2\right] \\ & + [\,R\left(\cos^2\tfrac{\varepsilon_r}{2} - \sin^2\tfrac{\varepsilon_r}{2}\right)\left(\cos\beta\cos\tfrac{\varepsilon_r}{2} - \sin\beta\sin\tfrac{\varepsilon_r}{2}\right) \\ & + 2R\sin\tfrac{\varepsilon_r}{2}\cos\tfrac{\varepsilon_r}{2}\left(\cos\beta\sin\tfrac{\varepsilon_r}{2} + \sin\beta\cos\tfrac{\varepsilon_r}{2}\right)]^2 \end{aligned} \tag{30}$$

Because in Eq. 1: $R \cos \beta = x$ and $R \sin \beta = y$, the value of $u_1^2 + u_2^2 - 2k^2$ can also be written as:

$$\begin{aligned} u_1^2 + u_2^2 - 2k^2 = {} & \left(\cos^2\frac{\varepsilon_r}{2} + 1 + 3\sin^4\frac{\varepsilon_r}{2}\cos^2\frac{\varepsilon_r}{2} + \cos^6\frac{\varepsilon_r}{2}\right)x^2 \\ & + \left(\sin^2\frac{\varepsilon_r}{2} + 1 + 3\sin^2\frac{\varepsilon_r}{2}\cos^4\frac{\varepsilon_r}{2} + \sin^6\frac{\varepsilon_r}{2}\right)y^2 \\ & + \left(8\sin^3\frac{\varepsilon_r}{2}\cos^3\frac{\varepsilon_r}{2} - 2\sin\frac{\varepsilon_r}{2}\cos\frac{\varepsilon_r}{2}\right)xy - 2r_1^2 \end{aligned} \tag{31}$$

For $\sin^4\frac{\varepsilon_r}{2}\cos^2\frac{\varepsilon_r}{2}$, $\cos^6\frac{\varepsilon_r}{2}$, $\sin^2\frac{\varepsilon_r}{2}\cos^4\frac{\varepsilon_r}{2}$, $\sin^6\frac{\varepsilon_r}{2}$, and $\sin^3\frac{\varepsilon_r}{2}\cos^3\frac{\varepsilon_r}{2}$ have little effect on the final result; Eq. 31 can be changed into:

$$\begin{aligned} u_1^2 + u_2^2 - 2k^2 = {} & \left(\cos^2\frac{\varepsilon_r}{2} + 1\right)x^2 + \left(\sin^2\frac{\varepsilon_r}{2} + 1\right)y^2 \\ & - 2\sin\frac{\varepsilon_r}{2}\cos\frac{\varepsilon_r}{2}xy - 2r_1^2 \end{aligned} \tag{32}$$

Now Eq. 20 can be written as:

$$x^2 + y^2 = \frac{r_1^2 + r_2^2 + R^2}{3} + \frac{(\cos^2\frac{\varepsilon_r}{2} + 1)x^2 + (\sin^2\frac{\varepsilon_r}{2} + 1)y^2 - 2\sin\frac{\varepsilon_r}{2}\cos\frac{\varepsilon_r}{2}xy - 2r_1^2}{3} \tag{33}$$

It can be changed into the following form:

$$\begin{cases} (2 - \cos^2\frac{\varepsilon_r}{2})x^2 + (2 - \sin^2\frac{\varepsilon_r}{2})y^2 + 2\sin\frac{\varepsilon_r}{2}\cos\frac{\varepsilon_r}{2}xy = R^2 + r_2^2 - r_1^2 \\ z = k \end{cases} \tag{34}$$

For $\left(\sin\frac{\varepsilon_r}{2}\cos\frac{\varepsilon_r}{2}\right)^2 - \left(2 - \cos^2\frac{\varepsilon_r}{2}\right)\left(2 - \sin^2\frac{\varepsilon_r}{2}\right) = 2\sin^2\frac{\varepsilon_r}{2} + 2\cos^2\frac{\varepsilon_r}{2} - 4 < 0$, the projection of the actual geometry of cylindrical control inserts with non-S shape involved in machining in x–y plane is ellipse [21]; thus, the 3-D tool nose geometry involved in machining is ellipsoid.

Figure 9 shows the actual geometry depicted by Matlab7.0 according to Eq. 34; both the major and the minor cutting edge radius are set to be 0.04 mm, and the tool nose radius is set to be 0.2 mm.

From Fig. 9, it can be seen that the middle space constituted by the two curve surfaces is an irregular ellipsoid, which gets good consistency with previous result that the 3-D geometry of cylindrical control with non-S-shaped tools is ellipsoid.

The solving process of conical control with non-S-shaped tool is similar to that of cylindrical control tools, and, by using the Cramer law to solve Eqs. 2, 13, and 15, the following relationship can be finally obtained.

$$\begin{cases} \sin^2\frac{\varepsilon_r}{2}x^2 + \cos^2\frac{\varepsilon_r}{2}y^2 + 2\sin\frac{\varepsilon_r}{2}\cos\frac{\varepsilon_r}{2}xy = r_2^2 - r_1^2 \\ z = -k \end{cases} \tag{35}$$

For $\left(\sin\frac{\varepsilon_r}{2}\cos\frac{\varepsilon_r}{2}\right)^2 - \sin^2\frac{\varepsilon_r}{2}\cos^2\frac{\varepsilon_r}{2} = 0$, the projection of the actual geometry of conical inserts with non-S shape involved in machining in x–y plane is parabola [21]. Thus, the 3-D geometry involved in machining is paraboloid.

5 Model validating

FEM simulation is conducted to validate the model based on the simulating of turning process and analyzing the

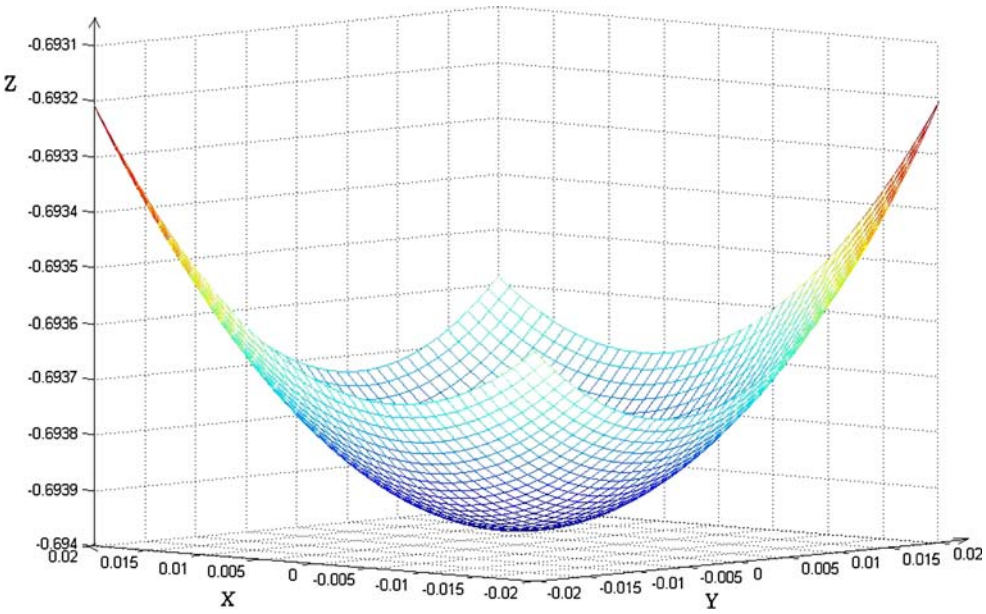

Fig. 9 Sketch map of the actual geometry direction

effects of tool geometry. The DEFORM 3-D simulation software is applied for the simulation. The material machined was AeroMet100. The FEM simulation was conducted by varying tool geometry, including CNMG 120404, DNMG110404, SNMG120404, and VNMG16 0404 and all of them were cylindrical control. The cutting speed is set to be 400 m/min; the feed rate is 0.05 mm/rev, and the depth of cut is 0.5 mm. During the simulation of the cutting process, the tool nose was involved in cutting to make sure that both the major cutting edge and the minor cutting edge were conducted in machining. Figure 10 shows the results of cutting force of the four tools. Figure 10a shows the force in X direction (axial force direction); Fig. 10b shows the force in Y direction (radial force direction), and Fig. 10c shows Z direction (tangential force direction).

It can be seen from Fig. 10 that the radial force (cutting force in Y direction) is the largest; tangential force (in Z direction) is the middle and axial force (in X direction) is the smallest which get good consistency with the conclusion in [10]. It can also be seen that cutting forces for C-, D-, and V-shaped tools are similar, whether in X, Y directions or in Z direction, while the cutting forces for S-shaped tool are smaller than those for the other three shape tools. The results can be explained by previous analyses that the actual geometry of cylindrical control of C, D, and V cutting tools involved in cutting is ellipsoid, and the actual geometry of S-shaped tools involved in cutting are sphere. When the actual geometry is ellipsoid, the contact area is larger than that of sphere, which makes heat dissipation better and in turn leads to lower cutting temperature. When the cutting temperature is reduced, the workpiece material begins to be hardened and finally leads to the increase in cutting forces.

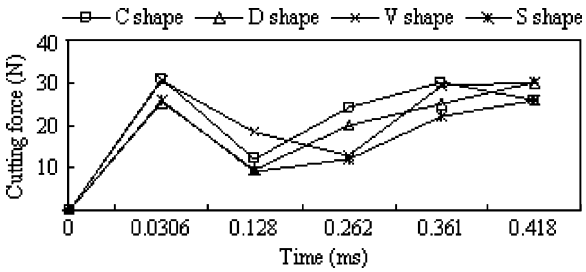

a. Cutting force in X direction

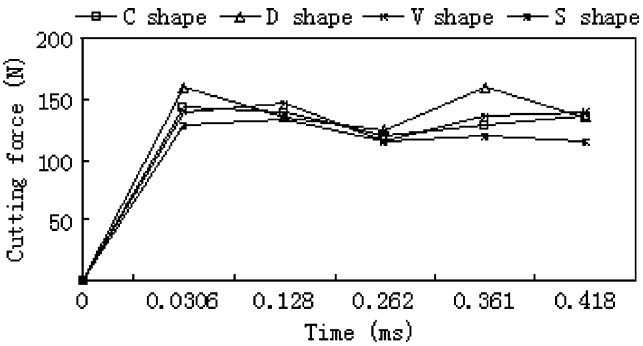

b. Cutting force in Y direction

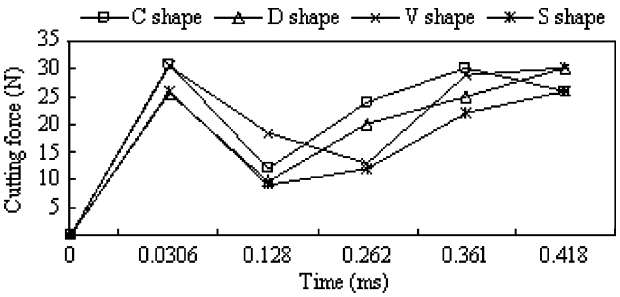

c. Cutting force in Z direction

Fig. 10 Cutting forces for four types of cutting tool. **a** Cutting force in X direction. **b** Cutting force in Y direction. **c** Cutting force in Z inserts

6 Summary and conclusions

Four different models have been developed to study the actual geometry involved in machining. These models are based on mathematics analytical methods including matrix translation and rotation. By analyzing these models, the following conclusions can be drawn:

1. The actual geometry involved in machining of the S-shaped inserts both with cylindrical control and with conical control is sphere.
2. The actual geometry involved in machining of non-S-shaped inserts with cylindrical control is ellipsoid.
3. The actual geometry involved in machining of non-S-shaped inserts with conical control is paraboloid.

Acknowledgements This project is supported by the National Natural Science Foundation of China (through grants no. 50675122 and 50828501), the National Basic Research Program of China (973 Program 2009CB724401), and the Natural Science Foundation of Shandong Province, China (through grants no. Z2007F03 and 2007ZCB01518).

References

1. Joshi SS, Melkote SN (2004) An explanation for the size-effect in machining using strain gradient plasticity. J Manuf Sci Eng 126:679–684. doi:10.1115/1.1688375
2. Hong SY, Ding Y, Jeong W (2001) Friction and cutting forces in cryogenic machining of Ti-6Al-4V. Int J Mach Tools Manuf 41:2271–2285. doi:10.1016/S0890-6955(01)00029-3
3. Barry J, Byrne G (2002) The mechanisms of chip formation in machining of hardened steels. J Manuf Sci Eng 124:528–535. doi:10.1115/1.1455643
4. Guo YB, Liu CR (2002) Mechanical properties of hardened AISI 52100 steel in hard machining processes. ASME J Manuf Sci Eng 124:1–9. doi:10.1115/1.1413775
5. Liu ZQ, Ai X, Zhang H (2002) Wear patterns and mechanisms of cutting tools in high speed face milling. J Mater Process Technol 129(1–3):222–226. doi:10.1016/S0924-0136(02)00605-2
6. Rodrigues AR, Coelho RT (2007) Influence of the tool edge geometry on specific cutting energy at high speed cutting. J Braz Soc Mech Sci Eng 29(3):279–283. doi:10.1590/S1678-58782007000300007
7. Thiele JD, Melkote SN (1999) Effect of cutting edge geometry and workpiece hardness on surface generation in the finish hard turning of AISI 52100 steel. J Mater Process Technol 94:216–226. doi:10.1016/S0924-0136(99)00111-9
8. Liu M, Takagi J, Tsukuda A (2004) Effect of tool nose radius and tool wear on residual stress distribution in hard turning of bearing steel. J Mater Process Technol 150:234–241. doi:10.1016/j.jmatprotec.2004.02.038
9. Chou YK, Song H (2004) Tool nose radius effects on finish hard turning. J Mater Process Technol 148:259–268. doi:10.1016/j.jmatprotec.2003.10.029
10. Özel T, Hsu TK, Zeren E (2005) Effect of cutting edge geometry workpiece hardness feed rate and cutting speed on surface roughness and forces in finish turning of hardened AISI H13 steel. Int J Adv Manuf Technol 25:262–269. doi:10.1007/s00170-003-1878-5
11. Chang CS, Tsai GC (2003) A force model of turning stainless steel with worn tools having nose radius. J Mater Process Technol 142:112–130. doi:10.1016/S0924-0136(03)00591-0
12. Huang Y, Liang SY (2003) Force modeling in shallow cuts with large negative rake angle and large nose radius tools application to hard turning. Int J Adv Manuf Technol 22:626–632. doi:10.1007/s00170-003-1550-0
13. Özel T, Karpat Y, Srivastava A (2008) Hard turning with variable micro-geometry PCBN tools. Ann CIRP 57:73–76. doi:10.1016/j.cirp.2008.03.063
14. Liu K, Melkote SN (2006) Finite element analysis of the influence of tool edge radius on size effect in orthogonal micro-cutting process. Int J Mech Sci 49:650–660. doi:10.1016/j.ijmecsci.2006.09.012
15. Komanduri R, Chandrasekaran N, Raff LM (1998) Effect of tool geometry in nanometric cutting: a molecular dynamics simulation approach. Wear 219:84–97. doi:10.1016/S0043-1648(98)00229-4
16. Rech J, Yen YC, Schaff MJ, Hamdi H, Altan T, Bouzakis KD (2005) Influence of cutting edge radius on the wear resistance of PM-HSS milling inserts. Wear 259:1168–1176. doi:10.1016/j.wear.2005.02.072
17. Chou YK, Evans CJ (1999) White layers and thermal modeling of hard turned surfaces. Int J Mach Tools Manuf 39:1863–1881. doi:10.1016/S0890-6955(99)00036-X
18. Ceretti E, Lucchi M, Altan T (1999) FEM simulation of orthogonal cutting serrated chip formation. J Mater Process Technol 95:17–26. doi:10.1016/S0924-0136(99)00261-7
19. Li R, Shih AJ (2006) Finite element modeling of 3D turning of titanium. Int J Adv Manuf Technol 29:253–261. doi:10.1007/s00170-005-2511-6
20. Rusnaldy, Ko TJ, Kim HS (2008) An experimental study on microcutting of silicon using a micromilling machine. Int J Adv Manuf Technol 39:85–91
21. Yao NX, Wang ZH, Chen ZJ (1988) Application of math in tool design. Mechanical Industry, Beijing